Neutron and Proton Spectra From Targets Bombarded by 450-MeV Protons*

J. W. Wachter, W. A. Gibson,† and W. R. Burrus†
Oak Ridge National Laboratory, Oak Ridge, Tennessee 37830
(Received 20 November 1968; revised manuscript received 23 August 1971)

The energy spectra of secondary neutrons in the energy region between 100 and 450 MeV emitted by targets bombarded by 450-MeV protons were measured using a proton-recoil spectrometer. Secondary-proton measurements were also made with this spectrometer. The measurements were made on Be, C, Al, Cu, Co, Pb, and Bi targets and at several angles between 0 and 60°. Two general target thicknesses were employed: thin targets in which the primary beam lost little energy and in which further interaction of the secondary particle was small; and thick targets in which the primary beam lost all or a significant fraction of the initial energy and in which the probability of the secondary particles undergoing further interaction was large. The thin-target results are expressed as cross sections and the thick-target results represent a nucleon transport and are expressed as a yield. A number of comparisons of the cross-section results against the Bertini intranuclear-cascade model indicate reasonable agreement for most secondary-proton data and some secondary-neutron data. In the latter case, the position of the observed quasifree scattering peak is at an unexpectedly low energy.

I. INTRODUCTION

In recent years several theoretical calculations have been made to predict the cross section for production of secondary particles in the interaction between high-energy nucleons and complex nuclei.[1-9] These calculations are based on models which involve assumptions that cannot be fully justified theoretically; therefore, justification relies heavily on comparisons with experiment. There are numerous experiments, particularly for secondary protons and mesons, with which checks can be made[10-14]; however, little data exist above 200 MeV which systematically cover certain parameters such as atomic weight, angle, or energy. To provide data which systematically cover a range of elements, angles, and incident energies for comparison with the calculations, a series of experiments has been performed to investigate the secondary-nucleon production in the interaction of primary protons bombarding complex nuclei.[15-17] The energy spectra of neutrons and protons presented here cover the region between 100 and 450 MeV from targets bombarded by 450-MeV protons and were measured for a number of elements ranging in atomic weight from beryllium to bismuth. Two categories of target thicknesses were studied: thin targets in which the primary beam lost little energy and the nuclear interaction mean free path is much larger than the target thickness; and thick targets in which the primary beam stopped or lost a large fraction of its energy and the target thickness was of the same order as the nuclear mean free path. The primary proton energy is well above the meson-production threshold and data should be of particular value for comparison with calculations which include meson production and its effects on the nucleon-production cross sections.

These measurements, made at the University of Chicago synchrocyclotron, are similar to those reported[17,18] for 160-MeV proton bombarding energy, and the data were recorded and analyzed using a proton-recoil spectrometer and analysis techniques similar to those employed in the 160-MeV measurements. In this paper, the experimental setup will be described only briefly with emphasis on the modifications to the previous spectrometer and analysis techniques. For details of the methods used to analyze the data, the reader is referred to Refs. 17 and 18.

II. EXPERIMENTAL SETUP

The proton beam from the synchrocyclotron was focused with two quadrupole magnets to a spot size of approximately 3 cm^2 on the target, as shown in Fig. 1, and the spectrometer was placed at the appropriate angle behind the target. By using stochastic beam extraction, a duty cycle of approximately 25% was obtained.

The energy of the beam was measured using a range telescope with Cu absorbers. Using the tables of Barkas and Berger[19] and applying the multiple-scattering correction of Janni,[20] the energy was found to be 450.4 ± 1 MeV. This corresponds to an effective range in Cu, including scintillators and light covers, of 144 g/cm^2.

The incident proton beam was integrated with helium-filled ion chambers[21] calibrated using the $^{12}C(p, pn)$ reaction.[22] To accomplish this calibration a plastic scintillator larger than the beam

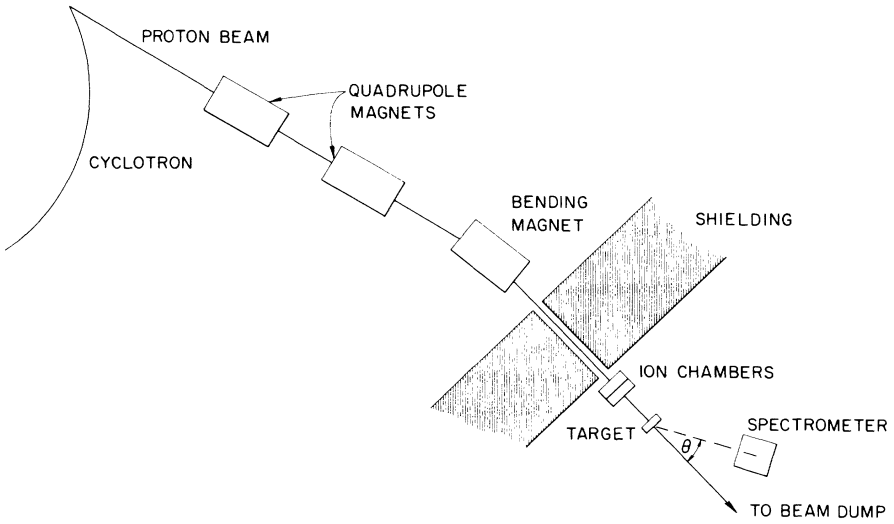

FIG. 1. Plan view of the experimental setup for measuring the neutron and proton spectra from targets bombarded by a 450-MeV proton beam.

spot was placed at the target position and exposed to the beam passing through the ion chambers. After exposure, the scintillator was placed on a photomultiplier tube and the activity induced by the $^{12}C(p, pn)$ reaction was calculated from the positron counting rate. The cross section used for this calibration was 32.3 mb. A correction was made for the positrons with energies below the counting threshold. This calibration was compared with the value obtained by extrapolating a calibration made using a 160-MeV proton beam monitored with a Faraday cup, and the two values were found to agree to within 5%.

III. SPECTROMETER

The measurements were made using the proton-recoil spectrometer shown in Fig. 2. The neutrons from the target impinged on the polyethylene radiator and the recoiling protons passed through the organic $\Delta E/\Delta X$ counter and produced pulses with a mean height

$$h \sim \int_0^T \frac{dl}{dE}\frac{dE}{dX}\,dX, \tag{1}$$

where dl/dE is the scintillation efficiency and T is the thickness of the counter. Since for protons dE/dX and dl/dE are monotonically decreasing functions of energy below approximately 2 BeV, the recoil proton energy may be determined from a measurement of pulse height. Figure 3 is a plot of the pulse height from the $\Delta E/\Delta X$ counter as a function of the energy of the protons incident upon the scintillator. The relationship was obtained by exposing the $\Delta E/\Delta X$ counter to protons of various

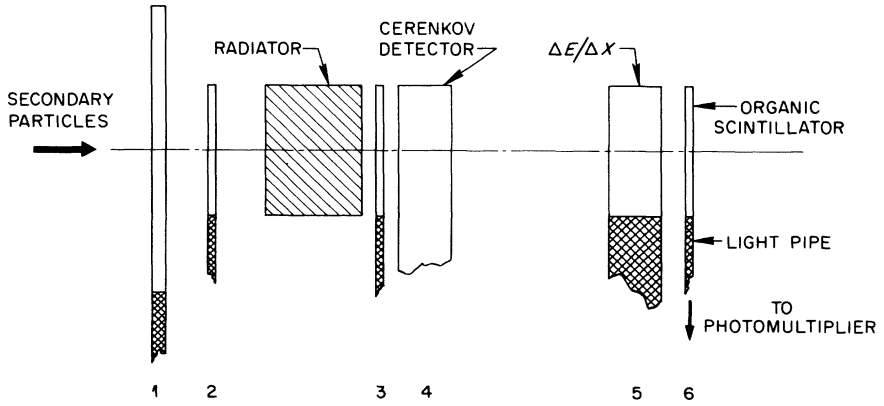

FIG. 2. Placement of counters and the hydrogenous radiator in the proton-recoil spectrometer.

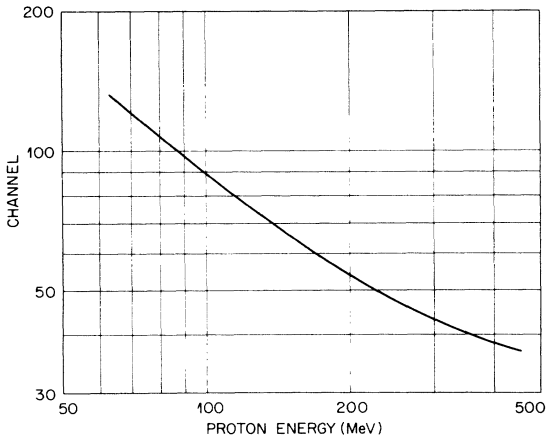

FIG. 3. Pulse height as a function of energy for protons traversing a 3.153-g/cm^2-thick plastic scintillator.

energies obtained by degrading the 450-MeV proton beam with copper absorbers. The energy E_p of the recoil proton is related to the energy E_n of the incident neutron by

$$E_p = E_n(\cos^2\theta)/[1 + (E_n/2Mc^2)\sin^2\theta], \qquad (2)$$

where θ is the angle between the path of the incident neutron and the recoil proton and M is the mass of a nucleon.

Counters 3 and 6 are placed in coincidence with the $\Delta E/\Delta X$ counter to reduce backgrounds from γ rays and neutrons. Counter 6 also ensures that recoil protons which do not penetrate the $\Delta E/\Delta X$ counter are not counted.

The counters in front of the radiator were placed in anticoincidence with the $\Delta E/\Delta X$ counter and served to reject counts due to protons present in the incident beam. In order to reduce the leakthrough in the anticoincidence channel due to the dead time caused by high random rates in the anticoincidence counters, two counters were employed in a "neither/nor" configuration. Background measurements were made by replacing the polyethylene radiator with a carbon radiator containing the same amount of carbon as the polyethylene radiator. Proton spectra were measured by removing the radiator and the anticoincidence requirements imposed by counters 1 and 2.

A severe background problem arose from mesons and high-energy electrons produced in the target and, in the case of neutron measurements, in the radiator. Due to the large resolution of

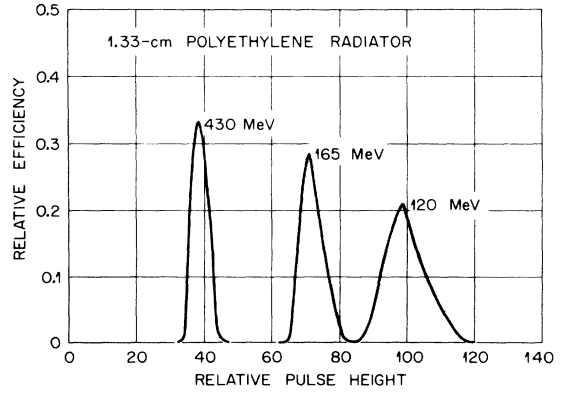

FIG. 4. Calculated pulse-height distributions for monoenergetic neutron beams incident on the spectrometer with the 1.33-g/cm^2 radiator. The calculation was made using the Monte Carlo technique discussed in the text.

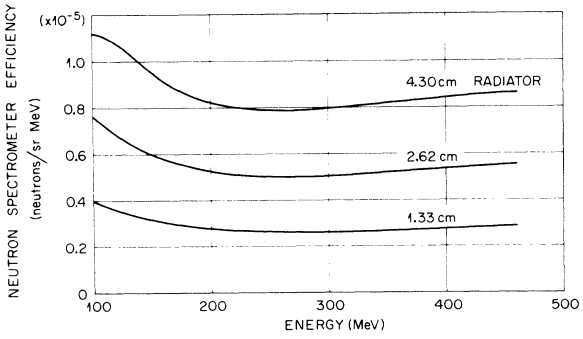

FIG. 5. Calculated neutron spectrometer efficiency for the polyethylene radiators used in the experiment. The calculation was made using the Monte Carlo technique discussed in the text.

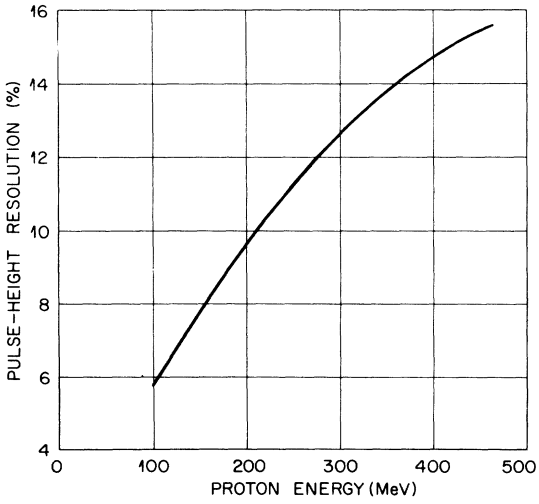

FIG. 6. Calculated pulse-height resolution as a function of energy for protons. In this case, the major contribution to the resolution was the energy-loss fluctuations in the $\Delta E/\Delta X$ counter and was the only effect included in these calculations.

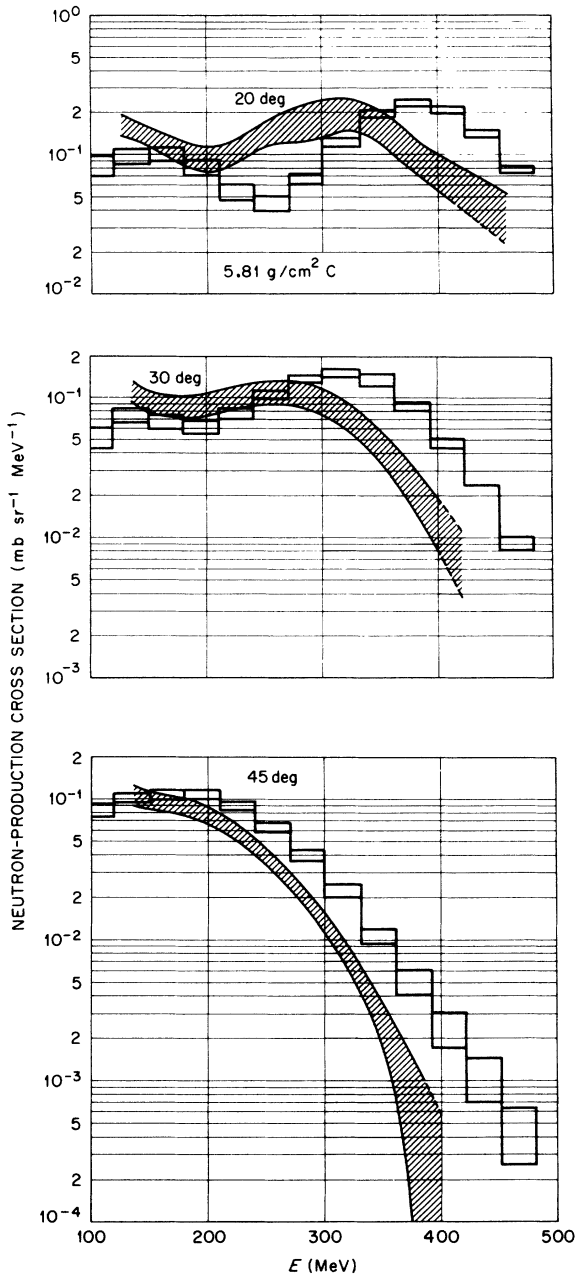

FIG. 7. Secondary-neutron-production cross section at 20, 30, and 45° for carbon bombarded by 450 MeV. The energy resolution associated with the spectra is Gaussian with a FWHM of 25%. The lines enclose the 68% confidence interval and include statistical uncertainties, uncertainties in calculating the efficiency of the spectrometer, and the degree to which the computer program is not able to fit the spectrometer response functions with the Gaussian energy resolution functions. The histogram is the calculated cross sections of Bertini smeared with a 25% Gaussian energy resolution so as to correspond to the energy resolution associated with the experimental results.

the spectrometer, many of the pulses produced in the $\Delta E/\Delta X$ counter by these particles were of the same size as the pulses produced by the high-energy recoil protons. In the case of the neutron measurements, the production of these background counts was somewhat different in the polyethylene radiator than in the carbon radiator, and these effects could not be entirely eliminated by a background subtraction. In the case of proton measurements, no background measurements were made for thick targets and the thin-target background measurements were made with the target out, resulting in an uncompensated residual background from the mesons and electrons. To reduce the number of these lighter particles which were counted, a Čerenkov counter with a threshold of $\beta = 0.67$ was placed in front of the $\Delta E/\Delta X$ counter and was connected in anticoincidence. An event $\overline{123}\overline{4}56$ was considered valid, and a multichannel analyzer was gated on and the pulse from the $\Delta E/\Delta X$ counter was stored.

The $\Delta E/\Delta X$ counter was a plastic scintillator,[23] 3.0 cm thick and 6.35 cm in diameter, optically coupled to the photomultiplier tube with a light pipe glued to the cylindrical edge of the scintil-

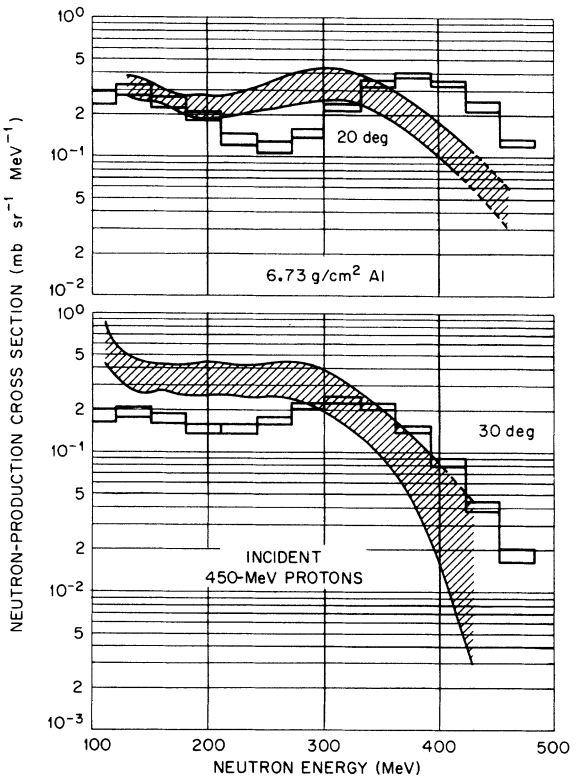

FIG. 8. Experimental and calculated secondary-neutron-production cross section at 20 and 30° for a 6.73-g/cm² aluminum target.

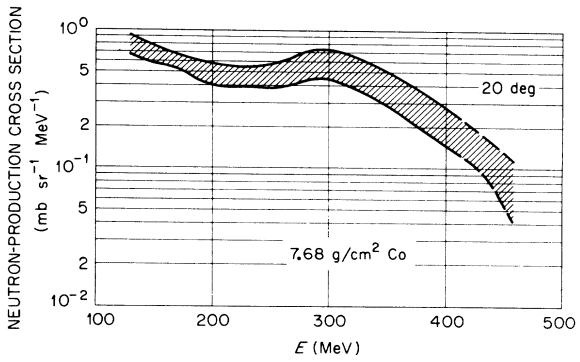

FIG. 9. Secondary-neutron-production cross section at 20° for a 7.68-g/cm^2 cobalt target.

lator. The uniformity of light collection was improved by painting the scintillator with white paint[24] and was found to vary less than 5% over the volume of the scintillator.

IV. DATA ANALYSIS

Important considerations in the design of the spectrometer are the pulse height and energy resolution. The resolution of a distribution is defined as:

$$R = \frac{\text{full width at half maximum of distribution}}{\text{centroid of distribution}}.$$

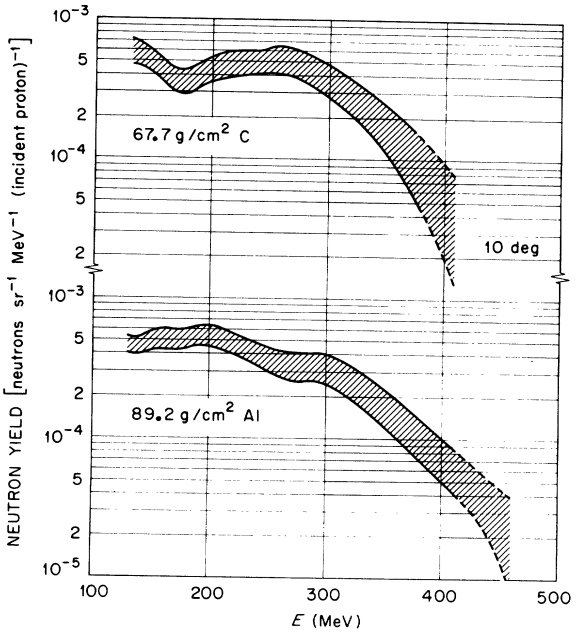

FIG. 10. Secondary-neutron-yield spectra at 10° to a 67.7-g/cm^2 carbon and an 89.2-g/cm^2 aluminum target.

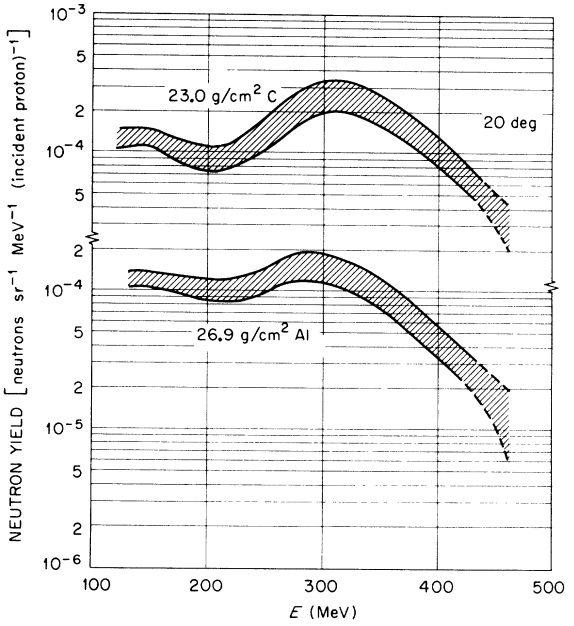

FIG. 11. Secondary-neutron-yield spectra at 20° to a 23.0-g/cm^2 carbon and a 26.9-g/cm^2 aluminum target.

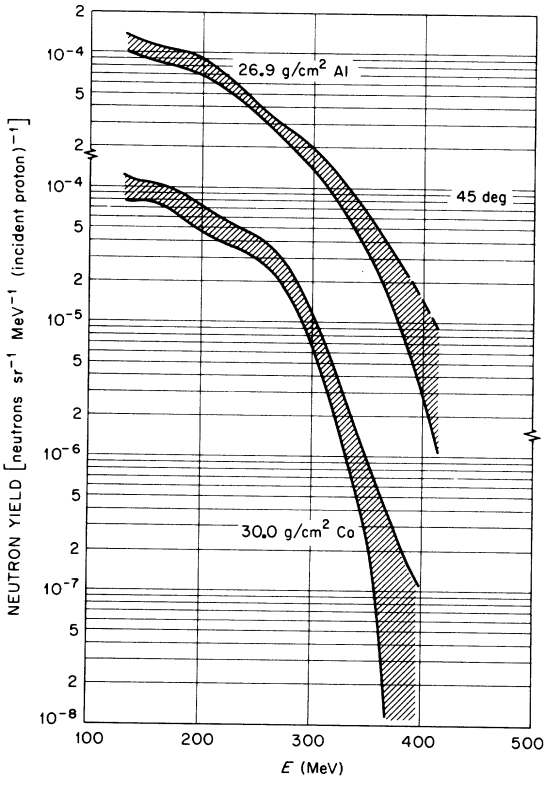

FIG. 12. Secondary-neutron-yield spectra at 45° to a 26.9-g/cm^2 aluminum and a 30.0-g/cm^2 cobalt target.

The pulse-height resolution of the spectrometer for neutrons is that of the distribution obtained by exposing the spectrometer to a monoenergetic beam of neutrons. The important factors determining pulse-height resolution are:
(1) the range of scattering angles between the neutron and recoil protons,
(2) the variety of energy losses in the radiator due to the various path lengths traveled by recoil protons,
(3) fluctuations of energy loss by the recoil protons in the $\Delta E/\Delta X$ scintillator.[25,26]

The energy resolution is defined as the resolution of the distribution obtained by transforming the above pulse-height distribution into an energy resolution using a one-to-one transformation between pulse height and energy. The contributions due to factors 1 and 2 can be readily controlled through the design of the spectrometer, and at the expense of efficiency can be reduced to small values. The contribution due to the third factor is determined by the thickness of the $\Delta E/\Delta X$ scintillator and decreases slowly with increasing scintillator thickness. For any reasonable choice of scintillator thickness the energy loss fluctuations for the higher energy protons were still large and were the determining factor on the practical resolution of the spectrometer. Due to the slow variation of dE/dX with proton energy at high proton energies, the energy resolution was considerably larger. The spectrometer was designed so that the combined contributions from factors 1 and 2 were somewhat less than the maximum from 3.

The data were analyzed using the simple-linear-

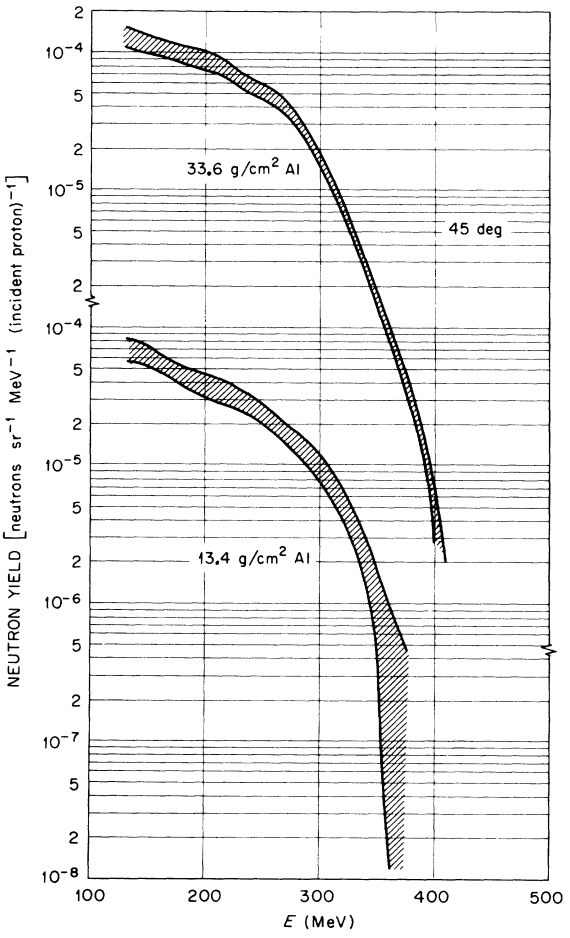

FIG. 13. Secondary-neutron-yield spectra at 45° to a 33.6- and a 13.4-g/cm² aluminum target.

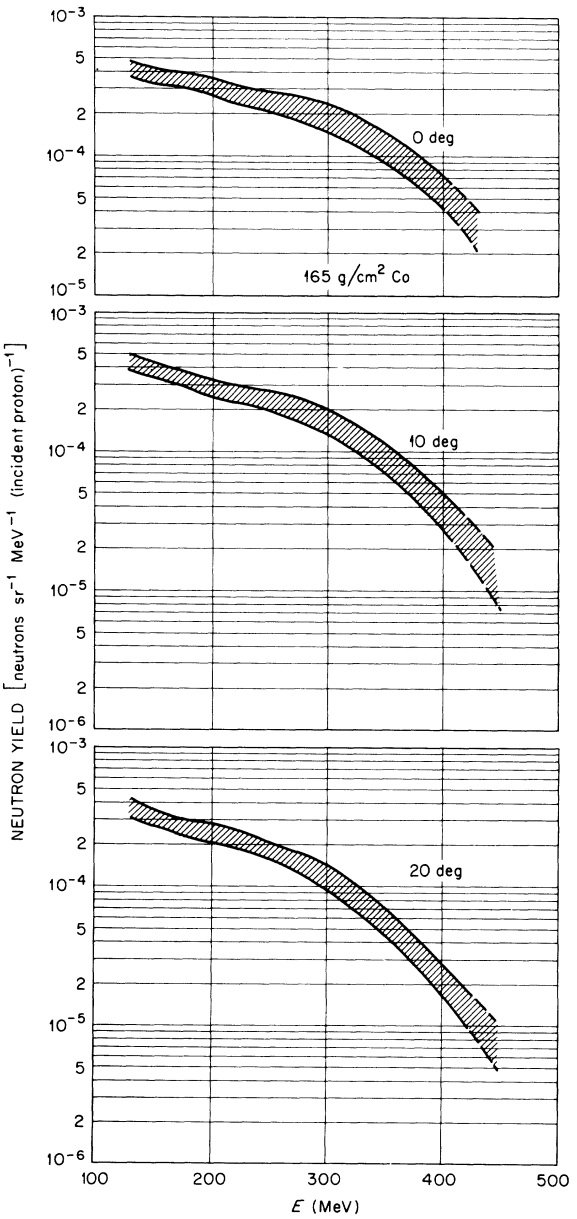

FIG. 14. Secondary-neutron-yield spectra at 0, 10, and 20° to a 165-g/cm² cobalt target.

TABLE I. Comparison of radiator thickness and mean proton energy loss in the radiator.

Radiator thickness (cm)	Energy of proton that loses 10% of its energy in radiator
1.33	100
2.62	150
4.30	200

optimization procedure (SLOP)[27] code in the manner described previously.[17, 18] Basically, the code is supplied with:

(1) the raw pulse-height data,

(2) the response functions of the spectrometer.

The response functions are the probability distributions that a particular energy particle will produce a pulse of a particular height.

Since it is not convenient to determine these distributions experimentally, they were calculated for the neutron measurements using a Monte Carlo code described previously[28] and combined with a calculation to incorporate the effect of energy loss fluctuations of the recoil protons in the $\Delta E/\Delta X$ scintillator. Typical results of this calculation are shown in Fig. 4. The total efficiency of the spectrometer for detecting neutrons was also calculated; the results for several different neutron energies are shown in Fig. 5. Proton-spectra measurements were made by removing the radiator and anticoincidence counters. In this case the response function is determined almost entirely by the energy loss fluctuations in the $\Delta E/\Delta X$ counter. However, in the case of the thin-target measurements in which the results are expressed as a cross section, the distribution of energy losses of the secondary protons in the target is included in the response function so that the results corrected to "zero-thickness targets." The pulse-height resolution of the spectrometer as a function of energy is given in Fig. 6 for protons.

The SLOP code calculates the range of energy spectra which is consistent with the raw data and the response functions. The energy response function associated with the output spectra is a Gaussian with a width specified by the user, and the results are presented in the form of a band which brackets the 68% confidence interval. The width of the confidence interval is determined jointly by the counting statistics, the uncertainty in determining the response functions, and the closeness of fit which is obtained between the desired Gaussian functions and a linear combination of the res-

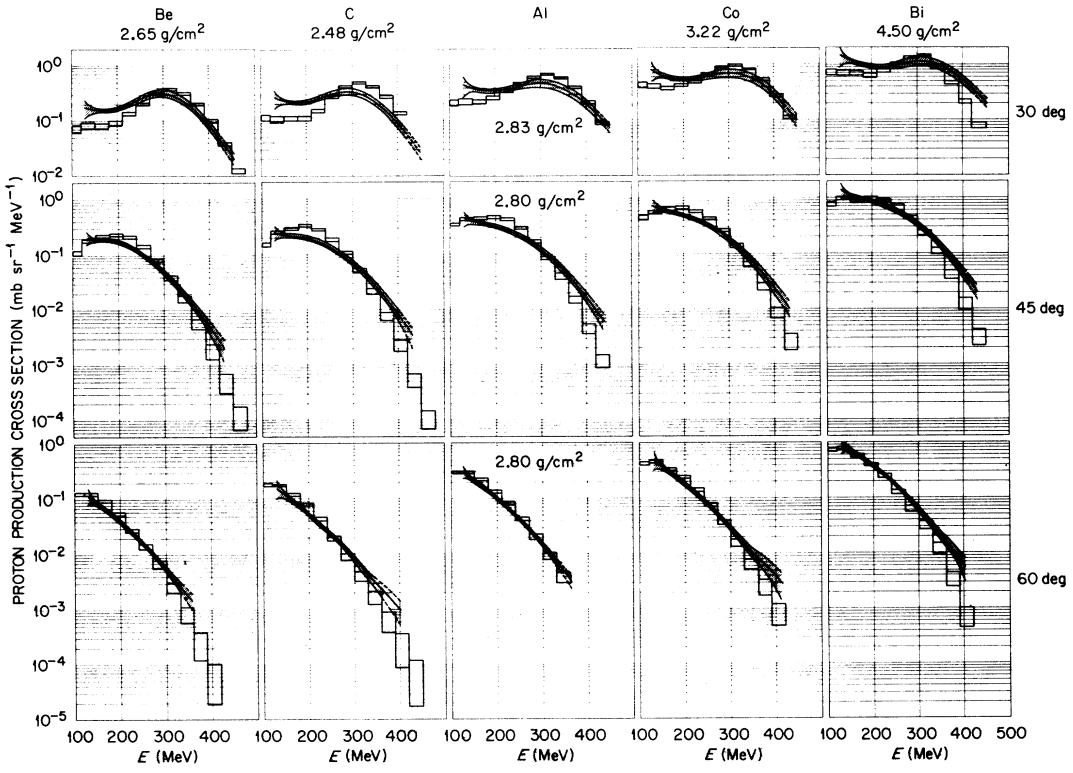

FIG. 15. Experimental and calculated secondary-proton-production cross sections for 30, 45, and 60° for various targets bombarded by 450-MeV protons. The histograms are the calculated cross sections of Bertini smeared with a 20% Gaussian energy resolution so as to correspond to the energy resolution associated with the experimental results.

ponse functions.

The resulting neutron and proton spectra were then adjusted to take account of the loss in number of protons detected at the final detector resulting from proton interactions with the materials of the telescope. These correction factors of 8 and 11% were calculated for the proton and neutron configurations using the tables of Measday and Richard-Serre.[29]

V. RESULTS

The neutron-spectrometer measurements on both thick and thin targets were obtained using polyethylene radiators with thicknesses listed in Table I. The spectral results are given in Figs. 7–14. Although in some measurements a 2.62-cm-thick radiator was used, most energy spectra were measured using both a 1.33- and a 4.30-cm-thick radiator and the results from these separate measurements combined in a statistically consistent manner to obtain the final energy spectrum. The energy resolution associated with these neutron-energy spectra is Gaussian with a full width at half maximum (FWHM) of 25%.

TABLE II. Parameters of neutron measurements.

Element	Thickness (g/cm^2)	Angle [a] (deg)	Distance to center [b] of target (cm)
		Cross sections	
Carbon	5.81	20	57.8
Carbon	5.81	30	57.7
Carbon	5.81	45	57.4
Aluminum	6.73	20	57.4
Aluminum	6.73	30	45.2
Cobalt	7.68	20	56.7
		Yields	
Carbon	67.7	10	75.7
Carbon	23.0	20	62.5
Aluminum	89.2	10	72.7
Aluminum	33.6	45	60.1
Aluminum	26.9	20	61.0
Aluminum	26.9	45	59.9
Aluminum	13.4	45	57.2
Cobalt	165	0	66.1
Cobalt	165	10	66.0
Cobalt	165	20	65.6
Cobalt	30.0	45	58.0

[a] The angles are measured between the primary proton beam line and the spectrometer axis. The targets were inclined so that a perpendicular to the target plane made an angle of 15, 22.5, and 30° to the beam axis for the spectrometer angles of 30, 45, and 60°, respectively. The beam, target, and spectrometer axes lay in the same plane.

[b] This distance is measured from the center of the target to the effective center of the radiators.

At high energies the effects of the γ rays and meson leak-through were evident in the final spectra, and in the cases where the distortion was large the high-energy portion of the graph was omitted. In the cases where the distortion was small the graph was extrapolated into the distorted region, as indicated by the dashed lines. At low energies the uncertainty in the spectra increased due to the large energy loss suffered by the recoil proton in the radiator and counters. The results were omitted in regions where the uncertainty was excessive.

Figure 7 shows the secondary-neutron-production cross section for a thin-carbon target at laboratory angles of 20, 30, and 45°. These data show a broad peak in the cross section that appears at about 320 MeV for the 20° data, and appears at lower energies and increasingly less pronounced at greater angles of observation. This peak is seen also in the 6.73 g/cm^2 aluminum shown in Fig. 8, although the peak is less well defined at either 20 or 30°. Similarly, in Fig. 9 the results from the 7.68-g/cm^2 cobalt target also show this peak.

This peak can be identified as due to the "quasi-elastic" scattering process and is characteristic of both the neutron and proton spectra taken at angles below 45°. It is attributed to a process in which the incident particle interacts directly with an individual nucleon within the target nucleus and the product nucleon would be expected to emerge with essentially the same energy and at the same angle as for an interaction between free nucleons. For light nuclei, the probability is high that the emerging nucleon does not undergo a further interaction with other target nuclei, and the peak is clearly defined. For heavy nuclei, these emerging particles interact with other nucleons and the peak is broadened, as seen in Figs. 7–9.

These data are compared with the cross-section predictions of Bertini.[30] Although based on semiclassical theory, the intranuclear-cascade model is the only one available at this time capable of handling more than one collision within the nucleus

TABLE III. Secondary-neutron-production cross sections above 120 MeV in mb/sr.

Angle (deg)	^{12}C	^{27}Al	^{59}Co
20	37.5 ± 8.6	72.2 ± 14.2	139.7 ± 31.0
30	22.1 ± 4.2	73.7 ± 22.1	...
45	11.2 ± 1.7	...	...

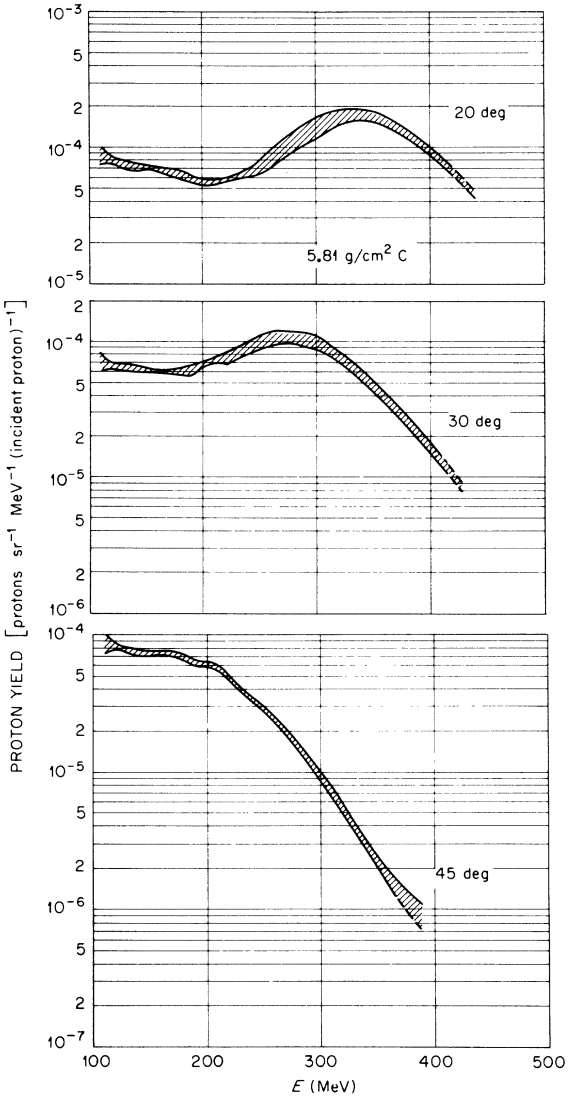

FIG. 16. Secondary-proton-yield spectra at 20, 30, and 45° from a 5.81-g/cm^2 carbon target.

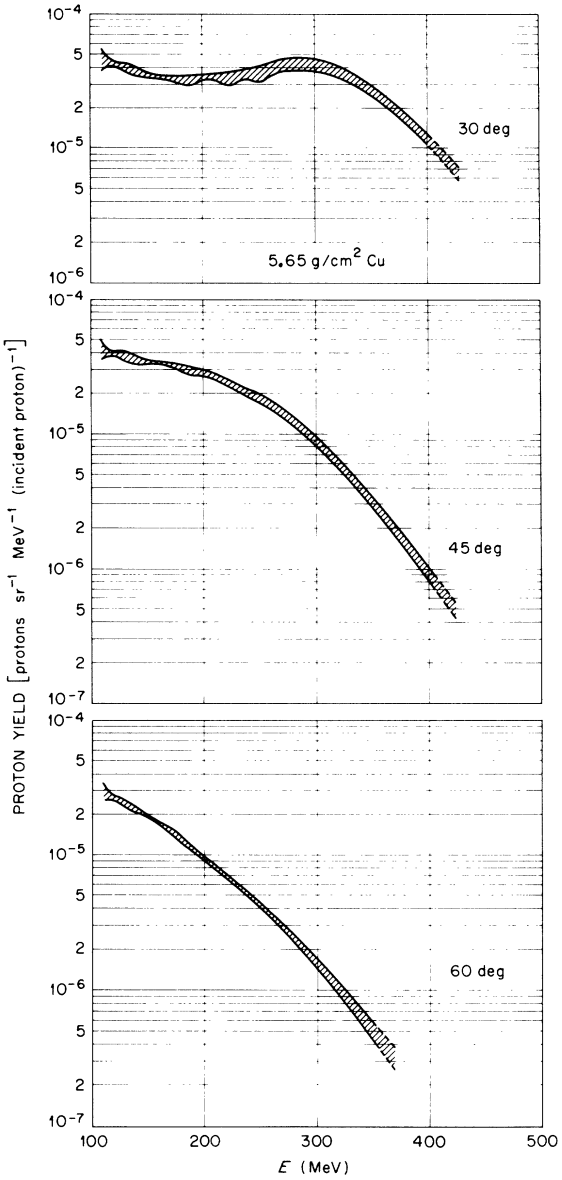

FIG. 17. Secondary-proton-yield spectra at 30, 45, and 60° from a 5.65-g/cm^2 copper target.

TABLE IV. Secondary-neutron-production yields above 120 MeV in neutrons $\times$ sr^{-1} $\times$ (10^3 incident protons)$^{-1}$.

Angle (deg)	^{12}C	^{12}C	^{27}Al	^{27}Al	^{27}Al	^{59}Co	^{59}Co
	Thickness g/cm^2						
	23.0	67.7	13.4	26.9	89.2	30.0	165
0	...	...	...	...	...	...	6.6 ± 1.1
10	...	56.7 ± 14.4	...	...	43.5 ± 7.2	...	47.6 ± 8.3
20	35.1 ± 8.2	...	...	27.6 ± 5.7	...	...	42.4 ± 6.8
45	...	...	11.9 ± 1.8	58.1 ± 11.0	...	10.6 ± 1.5	...
				10.0 ± 2.1			

so as to yield differential-secondary-particle spectra covering the whole energy and angle range. In this calculation the nucleons were assumed to move independently in a nucleus that had a three-region nucleon-density distribution approximating the distribution found by electron-scattering experiments. The nucleons were assumed to have a zero-temperature Fermi momentum distribution in each region. The interaction of the incident nucleon and the nucleons in the nucleus was considered to be a free-particle interaction. Using this model and the free-particle-interaction cross sections, the Monte Carlo program calculated the energy spectrum and angular distribution of particles emerging from the struck nucleus. The resulting spectra were smeared in energy by a 25% FWHM Gaussian distribution so as to permit comparison with the present data. The upper and lower 67% confidence limits of the calculated results are shown as histograms in Figs. 7 and 8.

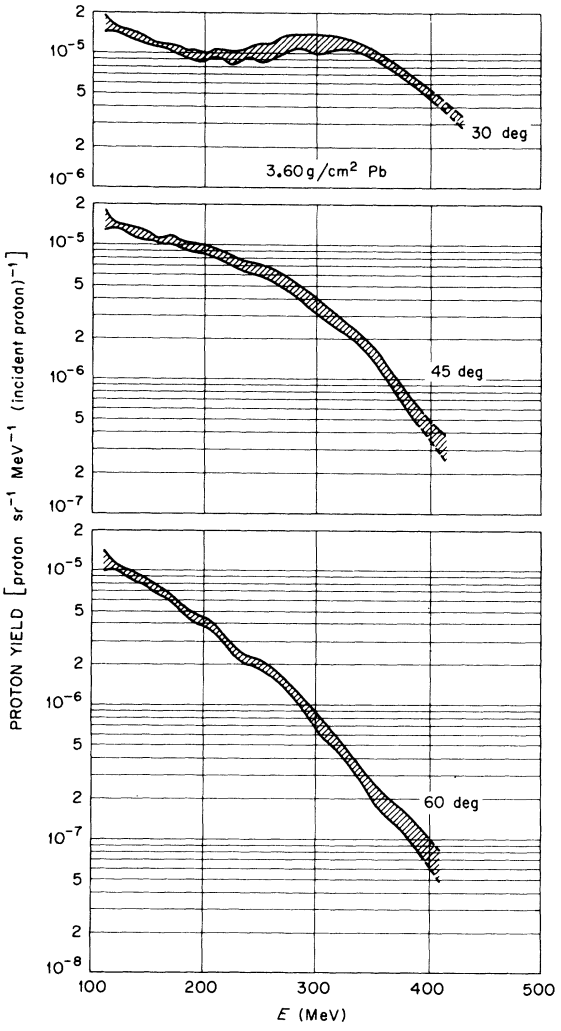

FIG. 18. Secondary-proton-yield spectra at 30, 45, and 60° from a 3.20-g/cm² lead target.

Thick-target secondary-neutron data are presented in Figs. 10–14. In these measurements the laboratory angle was measured between the incident-beam axis and the spectrometer axis at their point of intersection in the rear face of the target. The yield for all neutron energies was based on the calculation of spectrometer efficiency assuming all the particles were formed at the center of the rear face of the target. The distance from the center of the radiator to this point is given in Table II for each of the measurements.

Figure 10 shows the secondary-neutron-energy spectra for a 67.7-g/cm² carbon target and an 89.2 g/cm² aluminum target at an angle of observation of 10°. The primary protons lost approximately 200 and 240 MeV, respectively, in passing through these targets.

Figures 11 and 12 show neutron-yield spectra at 20 and 45° for targets in which a normally incident proton beam would lose approximately 60 MeV. In Fig. 13 the yields at 45° for aluminum targets of 33.6 and 13.4 g/cm² are compared.

In contrast to the "thin" targets, the larger energy loss of the incident proton beam within the target means that the observed particles include both secondary particles from interactions with incident protons of a wide range in energies and also tertiary particles.

Secondary-neutron production from a 165-g/cm² cobalt target is shown in Fig. 14 for angles of 0, 10, and 20°. This target thickness is about 14%

TABLE V. Parameters of proton measurements. The distance from the back counter of the spectrometer to the center of the back face of the target was 74.82 cm.

Element	Thickness (g/cm²)	Angles[a] (deg)
	Cross sections	
Beryllium	2.65	30, 45, 60
Carbon	2.48	30, 45, 60
Aluminum	2.80	30, 45, 60
Cobalt	3.22	30, 45, 60
Bismuth	4.50	30, 45, 60
	Yields	
Carbon	5.81	20, 30, 45
Aluminum	6.73	20
Copper	5.65	30, 45, 60
Cobalt	165	0
Cobalt	7.68	20
Lead	3.60	30, 45, 60

[a]This angle is measured from the center of the target to the effective center of the radiators.

TABLE VI. Secondary-neutron-production cross sections above 120 MeV in mb/sr.

Angle (deg)	Be	^{12}C	^{27}Al	^{59}Co	^{209}Bi
30	53.4 ±7.2	59.4 ±7.4	94.2 ±13.5	139.4±20.8	233.4±37.1
45	20.0 ±1.7	22.4 ±2.2	36.6 ±3.6	...	111.1±11.7
60	3.44±0.28	4.77±0.47	8.77±0.67	15.9±1.5	33.4±2.8

greater than the mean range of the incident proton beam.

Tables III and IV summarize the cross sections and yields obtained by integrating the above neutron-energy spectra above 120 MeV.

Measurements of secondary-proton production were made by removing the radiator and anticoincidence counters from the spectrometer. Proton cross-section measurements utilized targets in which the primary proton beam lost 6.7 MeV in traversing the target at normal incidence (see Table V). The calculated response functions took account of the energy loss of the secondary protons in the targets to produce cross sections corrected to "zero target thickness." The energy resolution associated with the spectra is Gaussian with a FWHM of 20%. Table VI and VII summarize the cross sections and yields obtained by integrating the proton energy spectra.

Figure 15 shows secondary-proton-production cross sections at angles of 30, 45, and 60° for various targets. For angles greater than 30° the target was turned through an angle of one-half the angle of observation about an axis passing through the same point. The quasielastic peak seen in the 30° cross-section data decreases in mean energy with increasing angle of observation and broadens with nuclear size.

The results of the Bertini-cascade calculation have been smeared in energy by a 20% FWHM Gaussian distribution and are shown as histograms defining the upper and lower limits of the calculations at the 68% confidence level. The agreement with the measurement is seen to be good, particularly for the elements of higher mass and for the wider angles of observation.

Figures 16–19 compare proton yields for several angles of observation from thick targets of C, Cu, Pb, Al, and Co. Since the low-energy secondary protons lost considerable energy in escaping the target, no attempt was made to include this loss in the response functions, and the spectra represent the energy of the protons as they leave the rear face of the targets. Although the 3.6-g/cm² Pb target was "thin," it had a nonstandard thickness, and therefore the data from this target are presented as a yield.

Figure 20 shows the proton yield at 0° from a 165-g/cm² cobalt target. Since the primary proton beam was completely stopped in this target, the observed yield is due to tertiary protons.

In those neutron data in which there is evidence for a quasielastic peak, the energy of the peak is lower than would be expected on the basis of a simple nucleon-nucleon interpretation. Such a calculation predicts that at lower energies and for 0° measurements the emerging nucleon, whether proton or neutron, can have essentially the energy of the incident proton. The peak as a function of angle should appear at energies given approximately by

$$T = E_0(\cos^2\theta)/[1 + E_0/2mc^2)\sin^2\theta] - V_0, \qquad (3)$$

where θ is the angle of observation, m is the mass of the nucleon, V_0 is an average nuclear potential of the nucleons at the point of interaction of the escaping nucleon, $E_0 = T_0 + V_0$, and T and T_0 are the kinetic energy of the emergent particle and the incident particle, respectively.

Data at higher energies for Be targets[31] show that the neutron peak at 0° also appears at a lower energy: 680-MeV protons produce a neutron peak at 610 MeV and 480-MeV protons show a neutron peak at 395 MeV. The internal beam of the cyclotron was used for these measurements so that

TABLE VII. Secondary-proton-production yields above 120 MeV in protons × sr^{-1} × (10^3 incident proton)$^{-1}$.

Angle (deg)	^{12}C	^{27}Al	g/cm²	^{59}Co	Cu	^{208}Pb
	5.81	6.73		7.68	5.65	3.60
6						
20	27.9±3.1	22.9±2.7		14.5±1.7		
30	16.3±1.5				7.7 ±1.7	2.3 ±0.3
45	5.4±0.3				3.2 ±1.2	1.1 ±0.1
60					0.85±0.04	0.40±0.02

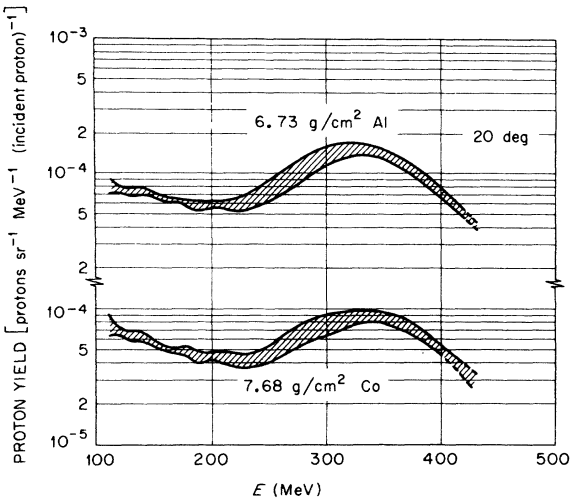

FIG. 19. Secondary-proton-yield spectra at 30, 45, and 60° from a 6.73-g/cm^2 aluminum and a 7.68-g/cm^2 cobalt target.

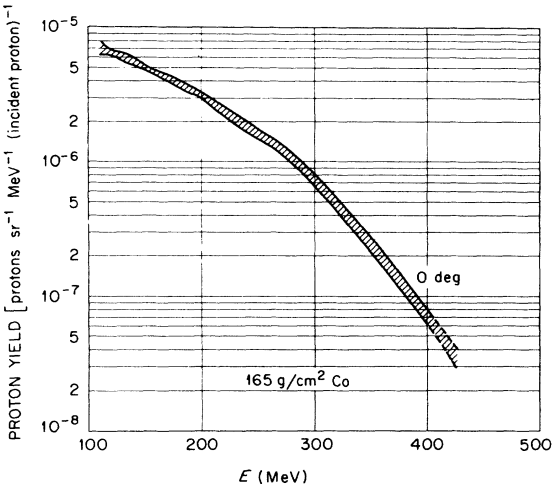

FIG. 20. Proton yield at 0° from a 165-g/cm^2 cobalt target. The primary proton beam was completely stopped in this target.

multiple traversal of the target by the bombarding protons was possible. The magnitude of the consequent energy reduction has been estimated by Kiselev and Fliagin[32] as 20 to 25 MeV. These data, therefore, indicate a net shift to lower energies of 55–60 MeV. Such a reduction in the neutron energy at 0° is consistent with the mean peak energies seen in the data reported here.

The effect of multiple scattering in broadening the peak and lowering the average energy have been estimated using the Bertini calculation at energies both higher and lower than that of this experiment. The calculational model does not consider coherent scattering, but does take account of successive incoherent scatterings with the target nucleons. Bertini[5] has compared the predicted proton spectra for 660-MeV protons on uranium resulting from the full Monte Carlo calculation with that obtained by looking at just those particles in the calculation which have undergone only a single collision. When multiple scattering is allowed, there is a filling in of the low energy part of the spectrum with a consequent shift in the mean peak energy. Wall and Roos[33] have used the Bertini calculation to study this effect in the quasi-elastic scattering of 160-MeV protons. They find that the full Monte Carlo calculation predicts significant multiple scattering even for targets as light as ^{9}Be.

Secondary-meson production also causes a reduction in the mean peak energy, particularly at the higher bombarding energies. Preliminary calculations using the Bertini Monte Carlo programs in which secondary-meson production was or was not included indicated that meson production must be taken into account in order to obtain correlation with the observed spectra.[34] The correlation with the proton thin-target data is seen to be good for the heavier elements at all angles of observation. The agreement is less good for the lighter elements and the agreement for C and Al targets at small angles is poor for both neutrons and protons.

These data cover a wide range of atomic number and angles and provide information to make detailed comparisons with stochastic calculations. Comparisons of the thin-target data with such calculations show qualitative agreement with theory; comparisons of the thick-target data for which a nucleon-transport code is required are reported elsewhere.[35]

VI. ACKNOWLEDGMENTS

The authors wish to thank the Physics Department of the University of Chicago and the Department of the Navy for making the synchrocyclotron available. The help of the synchrocyclotron staff is also appreciated. The aid of N. W. Hill of the Instrumentation and Controls Division at Oak Ridge National Laboratory in the design of electronics and in the performance of the experiment is gratefully acknowledged.

*Research partially sponsored by the National Aeronautics and Space Administration under Carbide Corporation's contract with the U. S. Atomic Energy Commission.

†Now with Tennecomp Inc., Oak Ridge, Tennessee 37830.

[1]M. L. Goldberger, Phys. Rev. 74, 1269 (1948).

[2]N. Metropolis *et al.*, Phys. Rev. 110, 185 (1958).

[3]V. S. Barashenkov *et al.*, Nucl. Phys. 14, 522 (1959/60).

[4]E. Abate *et al.*, Nuovo Cimento 22, 1206 (1961).

[5]H. W. Bertini, Phys. Rev. 131, 1801 (1963); Phys. Rev. 138, AB2(E) (1965); Phys. Rev. 188, 1711 (1969).

[6]K. Chen *et al.*, Phys. Rev. 166, 949 (1968).

[7]E. Gradsztajn, J. Phys. Rad. 24, 829 (1963).

[8]A. Avni *et al.*, Israel Atomic Energy Commission Report No. IA-975, 1965 (unpublished).

[9]J. P. Cohen, Nucl. Phys. 84, 316 (1966).

[10]K. Strauch and F. Titus, Phys. Rev. 104, 191 (1956).

[11]J. M. Cassels, T. C. Randle, T. G. Pickavance, and A. E. Taylor, Phil. Mag. 42, 215 (1951).

[12]J. B. Cladis, W. N. Hess, and B. J. Moyer, Phys. Rev. 87, 425 (1952).

[13]A. G. Meshkovskii *et al.*, Zh. Eksperim. i Teor. Fiz. 31, 987 (1956) [transl.: Soviet Phys. – JETP 4, 842 (1957)].

[14]L. S. Azhgirey *et al.*, Nucl. Phys. 13, 258 (1959).

[15]R. W. Peelle, T A. Love, N. W. Hill, and R. T. Santoro, Phys. Rev. 167, 981 (1968).

[16]W. Zobel, F. C. Maienschein, and R J. Scroggs, ORNL Report No. ORNL-3506, 1965 (unpublished).

[17]J. W. Wachter, W. R. Burrus, and W. A. Gibson, Phys. Rev. 161, 971 (1967).

[18]W. A. Gibson, W. R. Burrus, J. W. Wachter, and C. F. Johnson, Nucl. Instr. Methods 46, 29 (1966).

[19]W. Barkas and M. Berger, National Academy of Sciences–National Research Council Publication No. 1133, 1964, p. 103.

[20]J. F. Janni, Air Force Weapons Laboratory Technical Report No. AFWL-TR-65-150, 1966 (unpublished).

[21]R. T. Santoro and R. W. Peelle, ORNL Report No. ORNL-3505, 1964 (unpublished).

[22]J. B. Cumming, Ann. Rev. Nucl. Sci. 13, 261 (1964).

[23]NE-102 is manufactured by Nuclear Enterprises Ltd., Winnipeg, Canada.

[24]Water-base reflector paint, manufactured by Nuclear Enterprises Ltd., Winnipeg, Canada.

[25]B. Rossi, *High Energy Particles* (Prentice Hall, New York, 1952), Chap. 2, p. 22.

[26]D. M. Ritson, in *Techniques of High Energy Physics*, edited by D. M. Ritson (Interscience, New York, 1961).

[27]W. R. Burrus and V. V. Verbinski, Nucl. Instr. Methods 67, 181 (1969).

[28]W. E. Kinney and J. W. Wachter, ORNL Report No. ORNL-3499, 1963 (unpublished) p. 115.

[29]D. F. Measday and C. Richard-Serre, CERN Report No. CERN 69-17, 1969 (unpublished).

[30]Version MECC-3 of the Bertini cascade calculation was used and is described in Ref. 5.

[31]V. P. Dzhelepov *et al.*, Izv. Akad. Nauk SSSR Ser. Fiz. 19, 573 (1955) [transl.: Bull. Acad. Sci. USSR, Phys. Ser. 19, 514 (1955)].

[32]V. Kiselev and V. B. Fliagin, Zh. Eksperim. i Teor. Fiz. 32, 962 (1957) [transl.: Soviet Phys. – JETP 5, 786 (1957)].

[33]N. S. Wall and P. R. Roos, Phys. Rev. 150, 811 (1966).

[34]H. W. Bertini and J. W. Wachter, ORNL Report No. ORNL-4280, 1968 (unpublished) p. 148.

[35]R. G. Alsmiller, Jr., J. W. Wachter, and H. S. Moran, Nucl. Sci. Eng. 36, 291 (1969).